scientific reports

Check for updates

OPEN

Rake angle optimization for balanced efficiency and durability in PDC cutter cutting granite interaction via infrared thermal dynamics and fragmentation mechanism

Xiangjiang He[1], Bin Zheng[1✉], Zhecheng Luo[1], Peihao Hu[1], Yunjin Yang[1] & Guofu Yin[2]

In deep drilling operations, the interaction mechanism between the Polycrystalline Diamond Compact (PDC) cutter and the granite directly affects the granite breaking efficiency and the service life of the cutter. To reveal the correlation between the infrared radiation characteristics and the granite mechanics failure behavior during the single-tooth cutting process, the study utilized a modified shaper testing machine and a high-precision infrared thermal imager (with a measurement accuracy of ±0.01 °C and a spatial resolution of 0.6mrad) to monitor the dynamic contact process between PDC cutter and granite under the condition of 15° ~ 30° rake angles. The results show that the infrared temperature undergoes a significant increase at the moment of contact, and as the rake angle increases from 15° to 30°, the peak initial contact temperature rises from 26.30 °C to 91.46 °C, indicating that an escalation of the rake angle intensifies the degree of granite fragmentation but leads to an upward shift in the temperature fluctuation range at the contact interface, posing a potential threat to the durability of the PDC cutter. Infrared imaging analysis reveals that the granite fragmentation pattern exhibits the characteristics of diffusing from the local contact center to the circumferential direction, following a three-stage evolution law of energy accumulation, mixed failure, and unloading. By comparing the simultaneously collected cutting force data, it is found that the fluctuation of infrared radiation temperature is strongly correlated with the rock compaction-fracture cycle process, and the peak-valley changes in temperature highly coincide with the reciprocating characteristics of the cutting force waveband, verifying the feasibility of infrared thermal signals as real-time indicators of rock failure status. With the raise of the rake angle, the infrared characteristic temperature tends to decrease (mean is 39.54 at 30°, a decrease of 32% compared to 15°), while the variance significantly increases (variance is 21.34 at 30°, an increase of 48%), reflecting intensified energy dissipation but improved fragmentation stability during the granite breaking process. Comprehensive analysis of the Specific Energy of Rock Fragmentation (SERF) and cutting force reveals that when the rake angle exceeds 25°, the intensity of infrared radiation response, and cutting force increase simultaneously. Based on the principle of collaborative optimization of efficiency and service life, it is recommended to control the rake angle within the range of 15° ~ 25° to balance the granite breaking efficiency and cutter wear characteristics. This paper reveals the damage evolution law of granite to some extent.

Keywords PDC cutter, Rake angle, Granite breaking, Infrared thermal dynamics, SERF

In the field of deep drilling engineering, PDC cutters have become the core tool for breaking hard rocks such as granite due to their high hardness and wear resistance. As the development of oil and gas resources advance into

[1]School of Intelligent Manufacturing, Panzhihua University, Panzhihua 617000, China. [2]School of Mechanical Engineering, Sichuan University, Chengdu 610065, China. ✉email: 22198334@qq.com

nature portfolio

1

deeper strata, the interaction mechanism between PDC bits and granite has become increasingly significant in terms of rock-breaking efficiency, bit life, and project cost. How to precisely control the cutting parameters of PDC cutters to optimize the rock-breaking process while extending the service life of the bit has become a key scientific issue constraining the efficient progress of deep drilling projects. Infrared radiation technology, as a non-invasive monitoring means, can capture in real-time the energy conversion and thermal response processes of rocks under mechanical loading, providing a new perspective for revealing the micro-mechanical mechanism of PDC cutter cutting granite.

The essence of rock failure is a process of energy dissipation and transformation, a theoretical understanding that has promoted the application and development of infrared radiation technology. Early research used infrared radiation technology to measure the uniaxial loading process of red sandstone in real time, proposed the Average Cumulative Radiation Energy (ACRE) based on the Stefan-Boltzmann law, established a coupled mathematical model of elastic strain energy and ACRE, and successfully divided the rock failure process into four stages, compaction, elasticity, elastoplasticity, and failure[1]. The research confirms that the infrared radiation characteristics of rocks are highly correlated with their internal energy evolution, providing a theoretical basis for quantifying rock damage and predicting failure through infrared signals. However, the process of PDC cutter cutting granite involves complex conditions such as dynamic contact, local high temperature, and high strain rate, making it difficult for the research results under traditional uniaxial loading conditions to directly explain the thermal-force coupling mechanism in this process.

Study on the response characteristics of rock infrared radiation temperature to stress, providing an important reference for understanding the thermal phenomena in the cutting process. Stress tests on sandstone show that the infrared radiation temperature exhibits significant changes with different stress states. The maximal infrared radiation temperature can increase by 5 °C under compressive stress, and the minimal temperature can decrease by about 1.5 °C under tensile stress, with a nonlinear correlation between temperature and stress. These findings reveal the intrinsic relationship between the internal stress state of rocks and infrared radiation characteristics. However, when cutting granite with the PDC cutter, the stress distribution at the contact interface is highly non-uniform and transient, and existing studies have not fully explored the infrared radiation response patterns under such complex stress states[2].

In the field of rock damage monitoring and recognition technology, an important breakthrough has been made in the intelligent identification method based on infrared radiation. By constructing a deep convolutional neural network and analyzing the temporal and spatial evolution patterns of infrared radiation under different rock failure states, high-precision identification of rock damage states has been achieved, with an ACC index of 99.04% and a precision index of 99.39% on the validation set[3]. However, rock damage during PDC cutter cutting processes has characteristics such as dynamic evolution and multi-scale failure. The study on the influence of strain rate on the thermal infrared radiation characteristics of rocks shows that the infrared temperature change of rocks exhibits significant rate sensitivity under high strain rates. By using the Split Hopkinson Pressure Bar (SHPB) system found that when the strain rate exceeds a specific threshold, the infrared temperature change presents an allometric power function relationship with the strain rate[4]. When PDC cutters are used to cut granite, the strain rate in the contact area reaches up to $10^2 \sim 10^3 \ S^{-1}$, which is much higher than that in conventional loading tests.

In addition, the research on infrared monitoring of cracked rocks has proposed indicators such as the Number of Outlier Infrared Radiation Temperatures (NOIRT), and the visualization monitoring of the crack propagation process has been achieved through pixel grid analysis[5]. However, in the cutting process of PDC cutters, the rock fragmentation mode rapidly shifts from local crushing to overall disintegration, making it difficult for crack monitoring methods to capture this transient and dynamic failure process. The study of rock thermal infrared spectral characteristics provides a theoretical basis for understanding the thermal radiation phenomena during the PDC cutter cutting process[6]. Existing research has systematically analyzed the variation patterns of thermal infrared spectra in the 8.0 ~ 13.0 μm waveband for typical rocks such as sandstone, granite, and marble, discovering favorable wavebands corresponding to the static emissivity spectral Residual Features (RF) of different rocks, with the favorable waveband for granite located at 8.4 ~ 10.3 micrometers. In the rock fracturing stage, emissivity changes dominate the spectral radiance variations, while temperature changes exhibit anti-waveband characteristics. This property provides a scientific basis for analyzing the evolution of rock surface temperature fields through infrared spectroscopy. However, the high temperatures, high pressures, and transient stress changes at the contact interface make the rock's thermal infrared spectral response more complex. Existing research has not yet fully revealed the correlation between spectral characteristics and mechanical behavior under such conditions.

A multi-technology integrated rock loading stage prediction method provides a technical reference for studying the rock's mechanical behavior during the PDC cutter cutting process[7]. The traditional Acoustic Emission (AE) method is easily interfered with in complex engineering environments, while the new method combining Average Infrared Radiation Temperature (AIRT), and Convolutional Neural Network (CNN) achieves high-precision prediction of rock loading stages. Research shows that AIRT sequence fractal dimension first raise and then decreases in the elastic stage, and the water content significantly affects the fractal dimension changes at different loading stages. This multi-technology collaborative analysis framework provides an effective way to analyze the dynamic mechanical response.

The research of rock failure based on infrared radiation provides theoretical support for assessing the rock damage state during PDC cutter cutting processes[8]. By defining the Damage Infrared Response Matrix (DIRM) and the damage infrared energy response indicators, the study found that the indicators begin to rise in the stable crack growth stage of rocks and increases in the unstable crack growth stage. Therefore it can serve as a precursor indicator of rock failure. This result indicates that infrared radiation signals can effectively reflect the internal damage evolution process. However, rock damage has characteristics such as instantaneousness, multi-

scaling, and existing damage quantification methods still have shortcomings in capturing the dynamic damage evolution laws during cutting.

The infrared radiation study of pre-cracked rock masses reveals the influence of crack dip angles on rock failure modes[9]. The research findings show that as the dip angle of the pre-existing fissures increases, the rock mass failure mode transitions from tension-shear complex to tensile splitting, and the surface infrared radiation temperature exhibits a fluctuating characteristic of first decreasing and then increasing. This research based on pre-cracked fissures provides a reference for understanding the failure mechanism of rocks under localized stress concentration conditions. However, the stress distribution during the PDC cutter cutting process is more complex. The initiation and intersection of cracks are significantly affected by the dynamic changes of cutting forces, necessitating further study of the infrared radiation response characteristics under such conditions.

The development of rock infrared thermal image de-noising technology provides a guarantee for accurately acquiring the infrared signal during the cutting process[10]. In response to the problems of low contrast and poor signal-to-noise ratio in rock Infrared Thermal Image of Rock (ITIR), the proposed joint de-noising method for additive noise and multiplicative noise increases the Peak Signal-to-Noise Ratio (PSNR) of ITIR by 15.01% and the image quality score by 49.54%. However, in the high-speed dynamic process of the cutting process, how to further optimize the signal processing algorithm to achieve real-time and accurate extraction of infrared signals remains an urgent problem to be solved.

In the study of stress loading and rock burst processes, the collaborative analysis of infrared radiation and acoustic emission signals provides multidimensional information for disaster early warning. Research indicates that the infrared temperature of rocks increases linearly in the elastic stage, rises rapidly in the plastic stage, and exhibits a significant decrease before the occurrence of a rock burst. This anomalous temperature change, along with the decrease in the main frequency of acoustic emission signals, constitutes the precursory characteristics of a rock burst[11]. However, the rock failure during the PDC cutter cutting process is characterized by high frequency and dynamics, which is significantly different from static loading or rock burst processes, making it difficult to directly apply existing research results to the prediction of rock failure under cutting conditions.

Under the combined conditions of static ground stress and dynamic disturbance, an improved SHPB was used to conduct axial static pre-stress impact tests on sandstone at 0 ~ 75 MPa. By using high-speed photography to record the fracture process, dynamic parameters were obtained. The fracture mechanism of the comminuted samples was analyzed by combining displacement trend lines and digital image technology, and the fragment size was analyzed. The results show that with the same incident energy, the dynamic compressive strength first increases and then decreases with the increase of pre-stress, reaching a peak at 24.4% of the uniaxial compressive strength. The failure modes include intact, axial splitting, cracking, and comminution, with rock bursts occurring only under specific pre-stress and incident energy conditions. For comminuted samples, the increase in pre-stress will lead to changes in the fracture mechanism. High pre-stressed specimens release strain energy during the failure process, while low pre-stressed specimens absorb energy, indicating a positive correlation between the degree of crushing and pre-stress. The stress level is inversely proportional to the loading rate, providing a new approach for predicting rock fracture[12].

To sum up, this study is based on a modified bullhead planer experimental platform, using a high-precision infrared thermal imager to conduct in-situ monitoring of the dynamic process of PDC cutter cutting granite at the rake angle of 15° ~ 30°. The aim is to reveal the intrinsic relationship between infrared radiation characteristics and rock mechanics failure behavior. By analyzing the infrared temperature response, rock fragmentation patterns, and cutting force variation laws at different forward tilt angles, the energy dissipation mechanism under thermal-force coupling is quantified, and the optimization strategy for the PDC rake angle is proposed. The research findings will provide a theoretical basis for the design of PDC cutter geometric parameters, while expanding the application scope of infrared radiation technology in deep drilling engineering.

Experimental design
Sample Preparation
PDC cutter model used in the experiment is 1910, which means the diameter is 19 mm and the cutter body height is 10 mm. Four different types of rake angles were set, and they were welded on special tooth seats respectively for single-tooth cutting tests, as shown in Fig. 1.

Figure 1 shows the PDC cutter and their seat device used for single tooth cutting experiments. The left image shows four metal tooth sockets, each used for welding PDC cutter, providing a stable support for the experiment. The gear seat on the right is marked with four different rake angles of 15 °, 20 °, 25 °, and 30 °. These devices with angle markings are designed to investigate the effect of rake angles on the cutting performance of PDC cutter. By welding cutter with different rake angles onto specialized tooth seats, the relationship between rake angle and performance indicators such as cutting force, cutting efficiency, and wear can be systematically analyzed in single tooth cutting tests, providing experimental basis for the optimization design and application of PDC drill bits.

The rock material used for the test is granite, processed into a cuboid structure of $280 \times 200 \times 100$ in its natural state. A total of four rock samples were prepared, numbered HGY-1 to HGY-4.

During the experimental process, the determination of sample size strictly followed the theory of single tooth rock breaking. This theory provides a theoretical basis for sample size design by equivalently converting the rotational motion of the drill bit into linear motion, and the reserved size margin is sufficient to meet experimental requirements. To reduce experimental errors and avoid one-sided results, three repeated cutting tests were conducted for each rake angle condition, and the data of each test was recorded in detail. Ultimately, the key parameters such as cutting force and temperature field corresponding to each rake angle were analyzed based on a comprehensive comparison of multiple experimental data.

In addition, regarding the heterogeneity problem of rock samples, given that rocks are typical anisotropic materials, it is difficult to achieve complete consistency between their chemical composition and internal
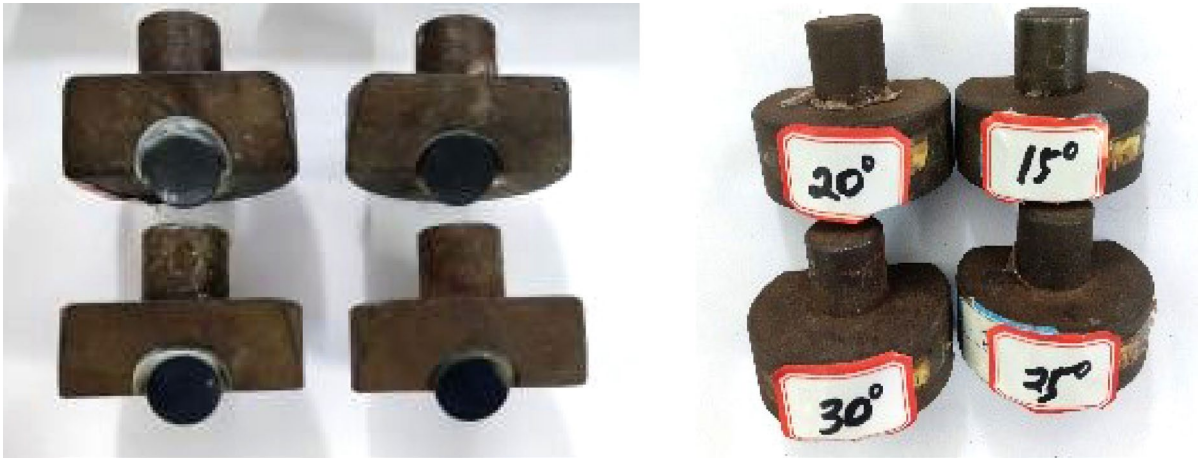
Fig. 1. PDC Cutter.

No.	Mass /g	Average diameter /mm	Cross-sectional area /mm²	Average height /mm	Volume /mm³	Density g/mm³	Average density /g/mm³
Granite 1	525	50.03	1965.25	100.26	197035.81	0.00266	
Granite 2	525	50.03	1965.25	100.35	197212.68	0.00266	
Granite 3	529	50.12	1972.32	100.77	198751.17	0.00266	0.00266
Granite 4	160	50.08	1969.18	30.67	60394.69	0.00264	
Granite 5	159	50.08	1968.79	30.41	59870.75	0.00266	

Table 1. Measurement parameters of the granite samples.

structure. To minimize the impact of this factor on the experimental results, the research team conducted uniaxial compression tests and Brazilian splitting tests on granite samples before officially conducting single tooth cutting tests. These two basic experiments not only obtained the basic physical parameters of rocks, but more importantly, through comparative analysis of experimental data, verified that the selected rock samples have relative consistency in physical properties, thus laying a solid foundation for the accuracy and reliability of subsequent single tooth cutting experiments.

Calibration experiment of basic physical parameters of the granite

Before conducting the single tooth cutting experiment, it is necessary to calibrate the parameters of the rock used in the experiment, with the main purpose of obtaining the basic mechanical parameters of the rock for subsequent analysis. Macroscopic mechanical parameters can be measured through uniaxial compression tests, Brazilian splitting tests, or shear tests on rocks. When PDC teeth break rocks, rocks usually undergo a mixed failure of tension and shear. Therefore, the research team will use uniaxial compression simulation, uniaxial tension simulation (Brazilian splitting), and shear simulation of rocks for parameter calibration.

According to national standards, the collected granite is processed into standard rock samples and their dimensions are measured. The steps are as follows.

Step 1: Diameter measurement. For cylindrical specimens, the vernier caliper is used to measure the diameter of their axial end faces and center position, and take the average of three sets of data as the final result. The same applies to disc specimens.

Step 2: Height measurement. For rock samples, the vernier caliper is used to measure three times around the top and bottom end faces in the axial position, at different positions on the plane, and take the average as the final result.

The statistical results are shown in the Table 1.

The uniaxial compression test of rocks (also known as the non-lateral confining pressure compression test) is the most commonly used rock strength testing test. The rock samples used in the experiment are usually cylindrical structures, and in order to reduce the influence of end effects, the ratio of length to diameter is generally 2 to 3.

There are two types of tensile failure tests for rocks, direct and indirect methods[13]. It should be pointed out that due to the relatively complex process of conducting direct uniaxial tensile tests on rocks and the difficulty in obtaining accurate data, indirect methods (i.e. Brazilian tests) are generally used in practical operations to determine the tensile strength of rocks[14].

The instrument used in the experiment is a microcomputer controlled electro-hydraulic servo universal testing machine (as shown in the Fig. 2), and the measurement process is strictly carried out in accordance with the national standard rock mechanics property testing regulations.
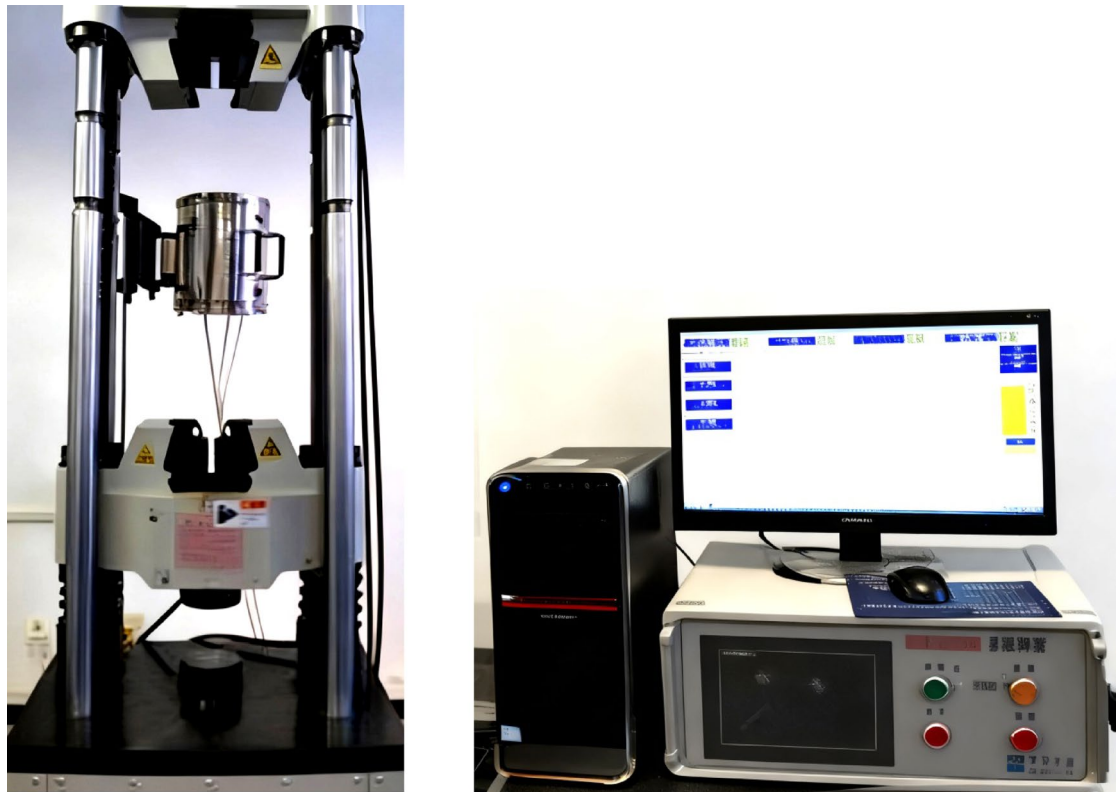
Fig. 2. Universal testing machine.

Fig. 3. Granite specimens after testing.

The basic physical parameters of the rock sample (including elastic modulus, Poisson's ratio, uniaxial compressive strength, and uniaxial tensile strength) are calculated by post-processing and analyzing the stress-strain curve and load displacement curve collected by the computer system during the experiment[15].

As shown in Fig. 3, the granite sample treated under specific experimental conditions exhibits obvious cracks on its surface, and the overall structural integrity is damaged to a certain extent.

Subsequently, in order to obtain uniaxial compression mechanical data of granite, according to the established experimental method, a microcomputer controlled electro-hydraulic servo universal machine was used to conduct uniaxial compression experiments on the finely prepared granite samples 1, 2, and 3. The experiment strictly followed the procedure, and the results were recorded in detail in Table 2.

Subsequently, in order to obtain the tensile properties data of granite samples No. 4 and No. 5, Brazilian splitting tests were conducted on these two groups of granite samples strictly following the established methods

No.	Elastic modulus /MPa	Mean elastic modulus /MPa	Poisson's ratio	Mean Poisson's ratio	Uniaxial compressive strength /MPa	Mean uniaxial compressive strength / MPa
Granite 1	13,589		0.21		73.04	
Granite 2	9054	11,816	0.29	0.25	64.79	71.04
Granite3	12,804		0.25		75.29	

Table 2. Uniaxial compression test results.

No.	Maximum load /N	Rock sample diameter /mm	Rock sample thickness /mm	Uniaxial tensile strength /Mpa	Mean average uniaxial tensile strength /MPa
Granite 4	8541.03	50.085	30.67	3.541	3.346
Granite 5	7534.25	50.080	30.41	3.151	

Table 3. Brazil splitting tests data results.

	Density/g	Elastic modulus/MPa	Poisson's ratio	Compressive strength/MPa	Tensile strength/MPa
Granite	0.00266	11816.21	0.25	71.04	3.346

Table 4. Basic mechanical parameters of the granite.

mentioned above. The entire experiment was operated in a standardized manner and recorded accurately. The final results are shown in Table 3.

After comprehensive analysis of the strength and deformation data obtained from uniaxial compression tests and the tensile data measured from Brazilian splitting tests, the basic physical parameters of the granite used in this experiment were finally summarized, as shown in Table 4.

Test process and methods

By using the modified shaper testing machine, single-tooth cutting tests were conducted, and piezoelectric sensors recorded the cutting forces generated during the test. An infrared thermal imager (Model: VarioCAM-HD) was used to monitor the thermal imaging of the rock sample surface[16]. The monitoring temperature limit of this infrared thermal imager is as high as 2000 ℃, which can accurately capture the surface temperature changes of rock samples in high-temperature environments. The measurement accuracy reaches ± 0.01 ℃, ensuring that subtle differences in the obtained temperature data are clearly presented. The spatial resolution reaches 0.6 ° mrad, which can effectively distinguish the thermal radiation differences in different areas of the rock sample surface. The image resolution is as high as 1024 × 768ppi, which can generate clear and detailed thermal imaging images, providing rich detailed information for subsequent analysis. In practical operation, in order to ensure that the infrared thermal imager can comprehensively and accurately record the infrared signals generated on the surface of the rock sample during the single tooth cutting process, the authors have carefully placed the infrared camera at a distance of about 0.5 m from the center of the rock placement after repeated debugging and optimization. This distance has been accurately calculated and verified through multiple experiments, ensuring that the infrared camera covers the surface of the rock sample completely, obtaining comprehensive thermal radiation information, and avoiding image distortion or signal attenuation caused by too close or too far distance. Therefore, it provides reliable and detailed experimental data for in-depth research on the thermodynamic characteristics of the rock sample surface during single tooth cutting process.

In this experiment, the calibration of the infrared thermal imaging instrument is crucial. The instrument is equipped with a corresponding calibration setting module, and before the formal experiment, the researchers conducted a pre experiment specifically. The core purpose of the pre experiment is to accurately explore the most reasonable temperature range during the cutting process[17]. Then, the key parameter is transmitted to the infrared thermal imaging instrument. By selecting the instrument settings parameters reasonably, it ensures that significant thermal infrared signals can be detected clearly and accurately. In addition, this experiment was conducted in an orderly manner under environmental conditions with a room temperature of approximately 15℃~20℃. Given that the temperature generated during the cutting process is much higher than room temperature, this significant temperature difference provides an extremely favorable objective environment for precise monitoring of experimental data, which helps to obtain high-quality and highly reliable experimental data.

In the actual experimental operation stage, the modified shaper testing machine is equipped with powerful sensors. After installing the fixture on the connecting shaft of the planer and before conducting the experiment, it is necessary to carefully inspect the force sensor and reset its data to zero to ensure the accuracy and consistency of the measurement starting state. During the cutting process, the force sensor and thermal infrared instrument jointly undertake the task of data monitoring. Two computers were set up on the experimental site, connected to the force sensor and thermal infrared instrument respectively, to achieve synchronous data recording. This

synchronous recording method effectively ensures the consistency of force signals and thermal infrared signals in the time dimension, providing a reliable basis for subsequent data analysis. In terms of data accuracy, potential errors mainly stem from delays in the electrical signal reception process. However, after actual measurement and evaluation, the delay time is extremely short, and its impact on the overall experimental results can be ignored, which will not cause substantial interference with the scientific and reliability of the experimental conclusions.

In the experimental design of this article, considering the feasibility of practical research and the effectiveness of data, the author conducted a series of pre experiments on the key parameter of cutting depth, setting different cutting depth values such as 0.5 mm, 1 mm, 1.5 mm, and 2 mm. The experimental results clearly indicate that a cutting depth of 1.5 mm is the optimal choice. When the cutting depth is insufficient, the effect of infrared detection is difficult to show clearly, and it is impossible to accurately obtain relevant thermal signal information. When the cutting depth is too deep, the modified shaper testing machine will experience axial vibration, which not only affects the stability of the experimental equipment, but also poses certain safety risks. In addition, based on the research data of the depth of each rotation of the drill bit during the actual drilling process, after comprehensive consideration, it was finally determined to use a cutting depth of 1.5 mm for subsequent experiments. In this cutting experiment, four different types of PDC cutter with different rake angles were specially set up to explore the influence of rake angles on cutting effects. At the same time, the cutting depth was fixed at 1.5 mm and the straight cutting distance was set at 200 mm to ensure the consistency of experimental conditions and facilitate comparative analysis of test results under different rake angles. The experimental platform with relevant equipment installed is shown in Fig. 4.

After the test equipment is set up, let it stand for 5 min to allow the temperature of the test piece to reach equilibrium with the ambient temperature, ensuring the accuracy of the recorded data.

Analysis and discussion of experimental results
### Infrared radiation characteristics of tooth and rock contact area
Based on the rock loading conditions, the development of micro-fractures will cause changes in the infrared temperature of the rock surface[18]. Therefore, the intensified development of rock micro-fractures before rupture may lead to abrupt changes in its infrared temperature. Unlike conventional uniaxial compression tests, rocks begin to break at the initial contact moment when the cutting test starts.

The IRBIS 3 Professional software is used to perform infrared thermal imaging analysis on the rock cutting process of PDC cutting tools, as shown in Fig. 5. This image accurately presents the dynamic temperature field distribution characteristics of the tool rock contact area during the cutting process through thermal radiation data visualization technology. Among them, the color code on the right uniformly adopts a Celsius (° C) scale, ranging from 12° C (black) to 38° C (red and white), and intuitively reflects the temperature through color gradients (black, gray, purple, blue, green, yellow, orange, red and white). The closer the color is to red and white, the higher the temperature is.
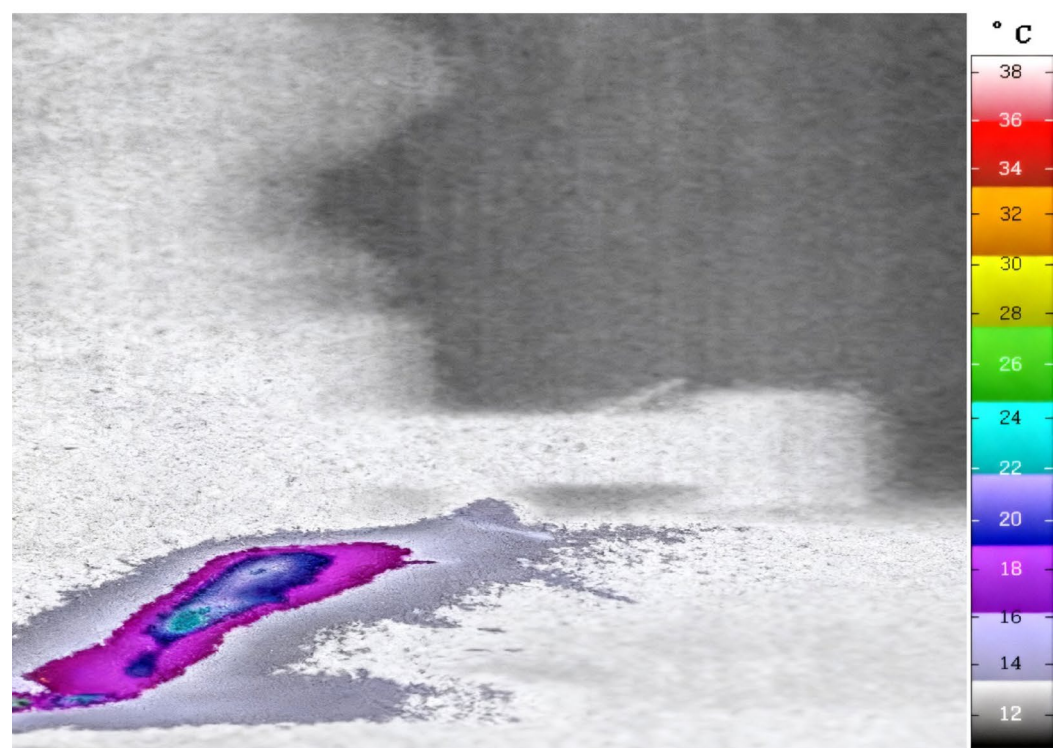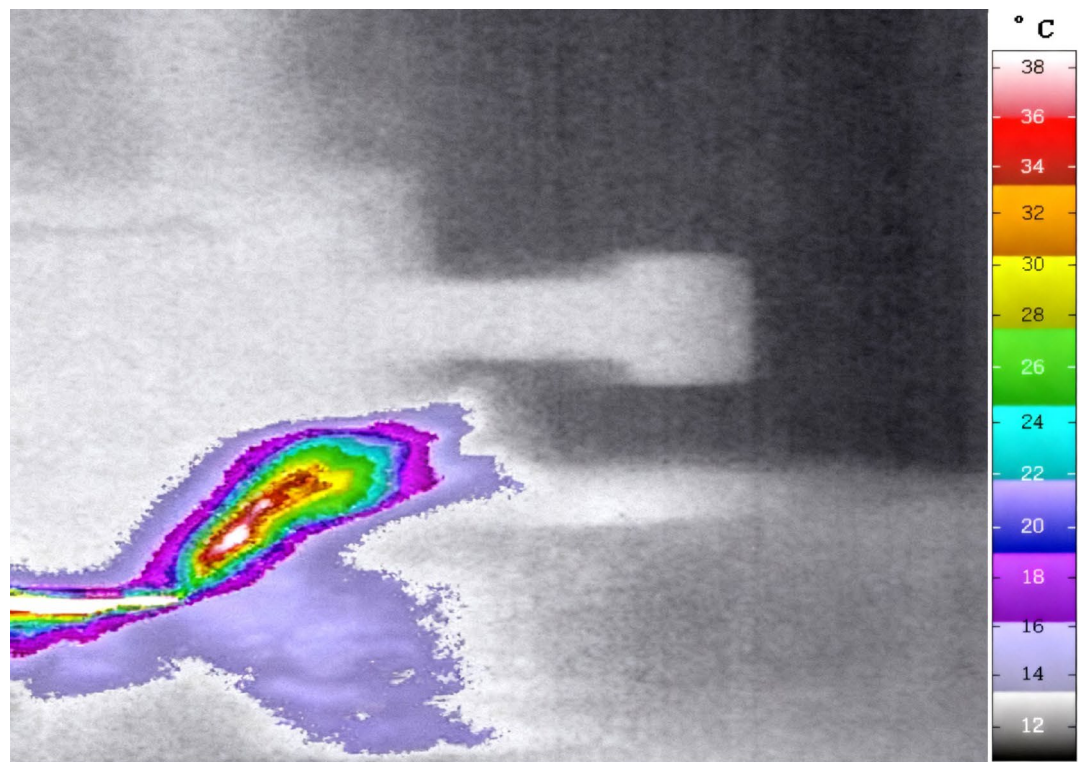

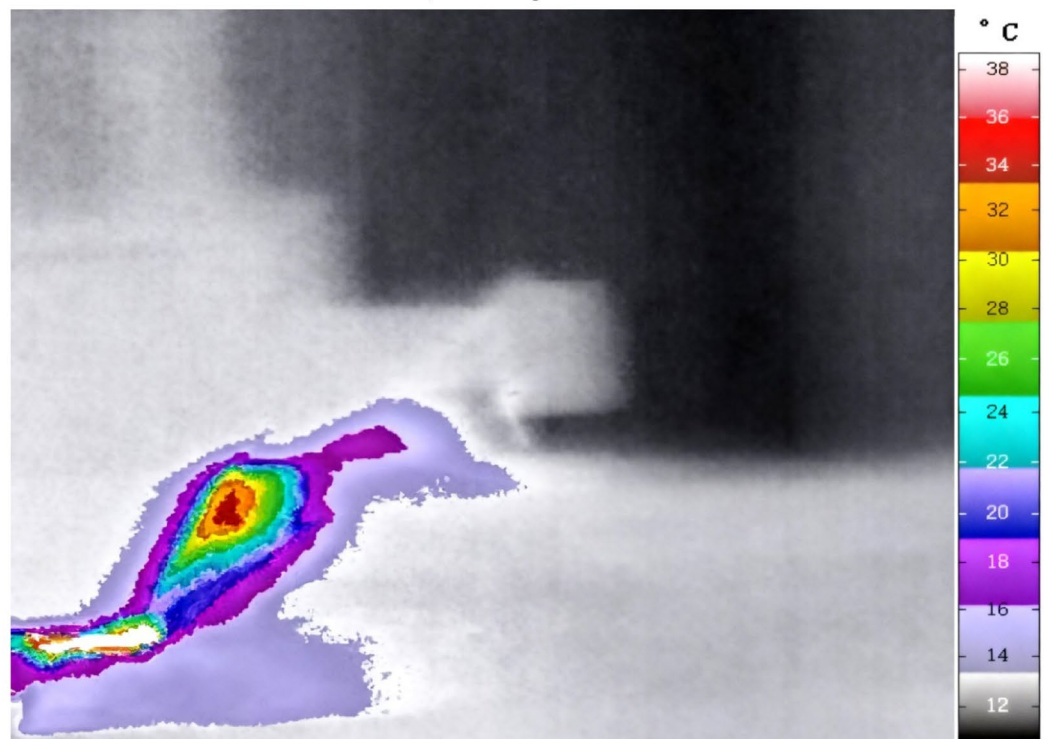**Fig. 4.** Cutting test machine.
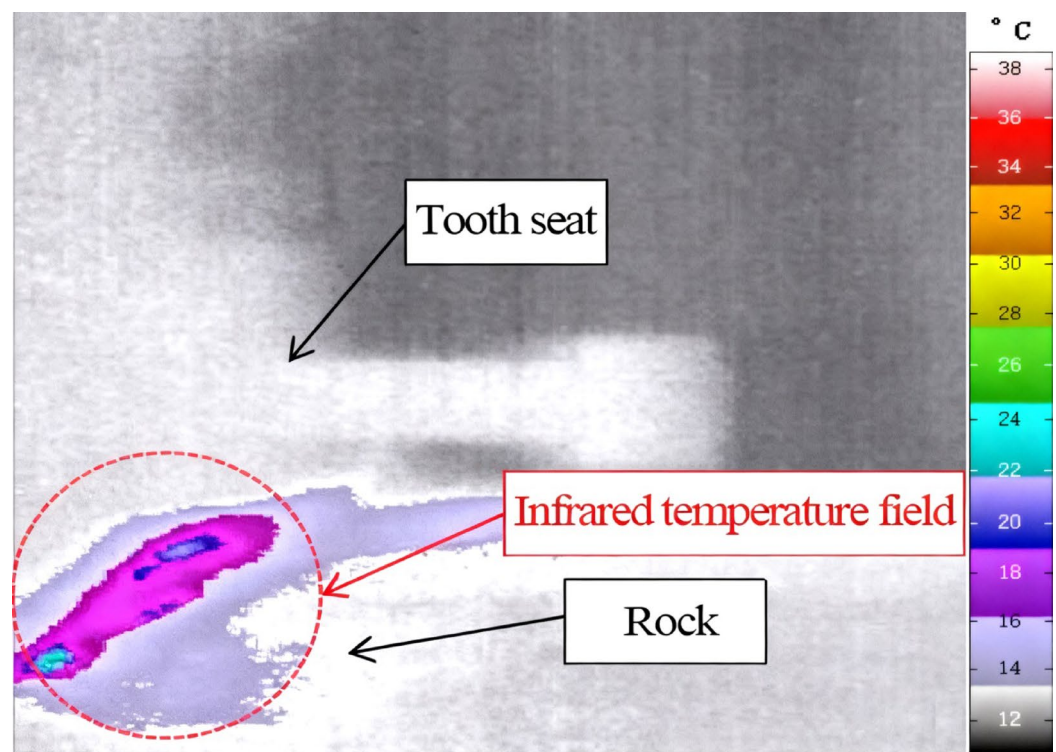
a) Rake angle is 15°.

b) Rake angle is 20°.

Fig. 5. Initial contact temperature distribution at different rake angles. (**a**) Rake angle is 15°. (**b**) Rake angle is 20°. (**c**) Rake angle is 25°. (**d**) Rake angle is 30°.

c) Rake angle is 25°.

d) Rake angle is 30°.

Fig. 5. (continued)

The Tooth seat in the figure is the installation component of the cutter, the Rock is the object to be cut, and the Infrared temperature field shows the temperature distribution area of the rock and its surroundings during the cutting process. It can be observed that the cutting area presents a clear color temperature gradient. The color range and shape of the temperature field vary in different figures, reflecting that during the cutting process,

as the cutting action progresses, the distribution of the temperature field and the position and range of the high-temperature area continue to change. These changes can be used to study the heat generation and transfer laws of PDC cutter when cutting rocks, providing a basis for optimizing cutting parameters, improving cutting efficiency, and tool life.

It is not difficult to see that during the cutting process, an obvious infrared radiation signal is generated in the area where the PDC tooth contacts the rock, which can characterize the fragmentation of the rock. To explore the laws and connections contained therein, the infrared signals of the PDC tooth contacting the rock throughout the entire process were extracted, as shown in Figs. 6 and 7.

Figure 6 shows the experimental setup and thermal imaging results of infrared temperature monitoring during the process of PDC cutter cutting rocks. Regarding the upper part of Fig. 4, the PDC cutter is a tool used for cutting rocks. The infrared temperature monitoring array is used to monitor the temperature of the cutting area. Cut rock refers to rock that has been cut. Uncut rock refers to uncut rock that has not been cut, which clearly distinguishes the different states of the rock. The red dots and black branches indicate the cutting action area.

The infrared thermal imaging image of the lower part presents temperature distribution with color gradients of blue, yellow, red, etc. The more inclined the color is towards red and yellow, the higher the temperature. The red dashed box in the figure corresponds to the infrared temperature monitoring array in the upper part, showing the high temperature distribution in the cutting area, which intuitively reflects the heat generation and distribution of PDC cutter during rock cutting. It can be used to analyze the thermal behavior during cutting and provide a basis for optimizing cutting parameters and studying tool thermal wear.

The results show that as the rake angle is 15°, the maximal infrared temperature value at the initial contact moment between the PDC cutter and the rock is the lowest, only 26.30 °C. As the rake angle increases, the measured maximum infrared temperature also increases, reaching 91.46 °C at 30°. It can be seen that at the initial contact moment between the PDC cutter and granite, the infrared temperature undergoes significant changes, followed by the corresponding granite beginning to break. As the rake angle increases, the infrared temperature shows a significant upward trend. This indicates that the fragmentation of granite becomes more intense. After the cutting edge contacts the rock, in addition to the sharp change in infrared temperature within the effective contact area of the PDC cutter cutting granite, there is also a weak change different from the ambient temperature on the surface of the granite around the contact area. This is because after the rock breaking begins,
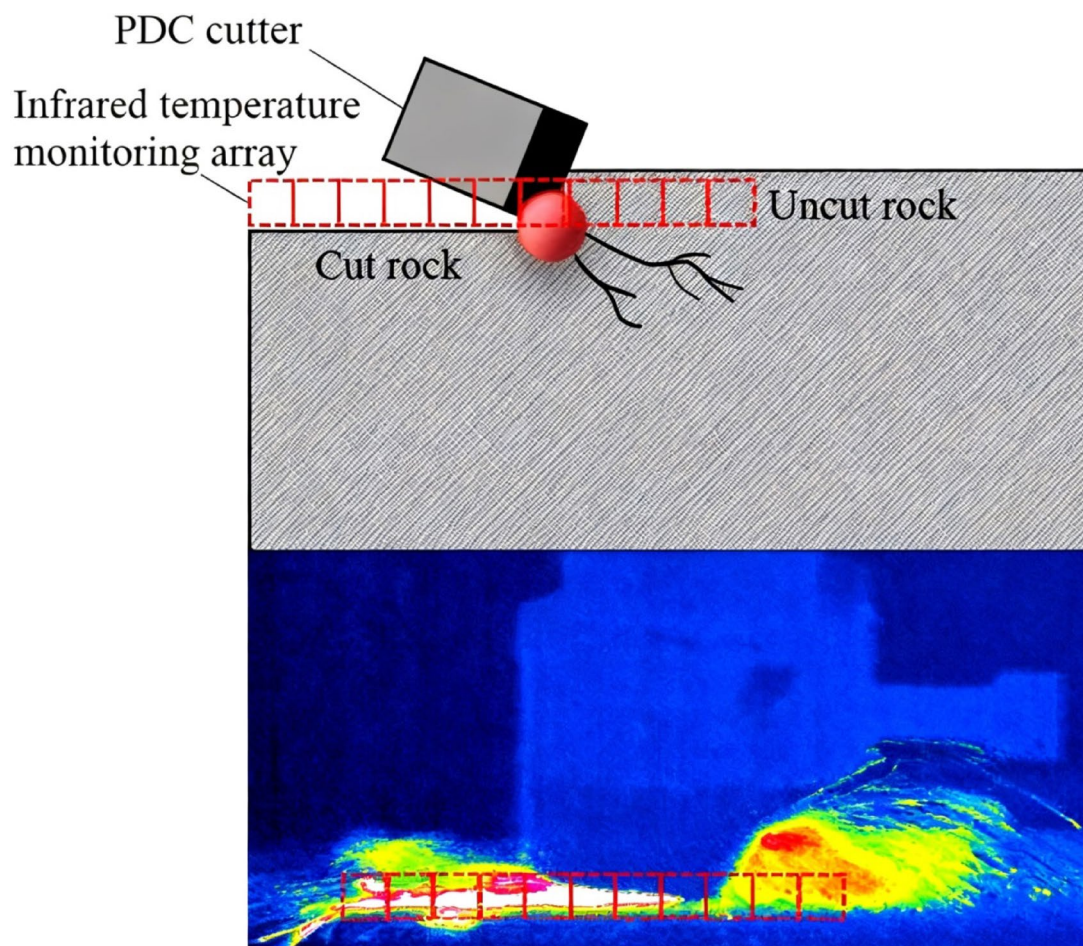
Fig. 6. Infrared temperature monitoring of the contact area between the tooth tip and the rock.
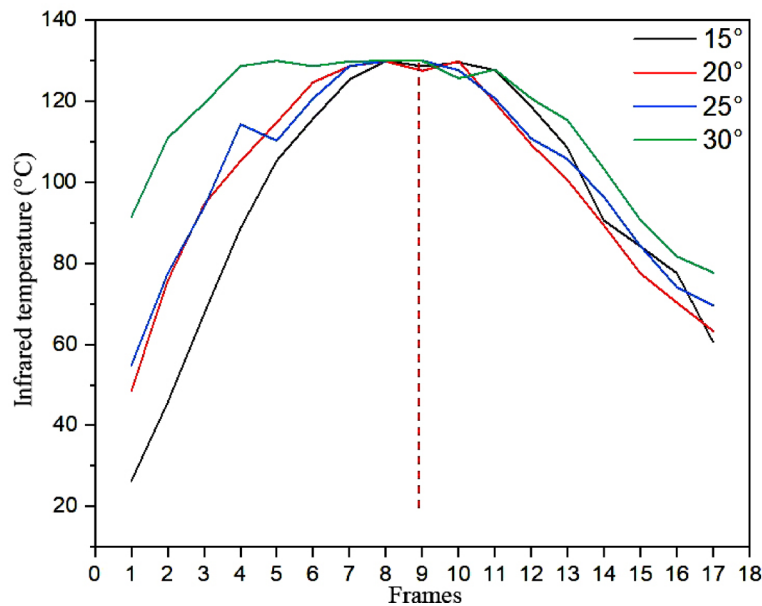
Fig. 7. Infrared temperature response of PDC tooth to rock contact area under different rake angles.

the fragmentation of the rock is not only reflected in the central contact area but also spreads to its surroundings, and complex structural changes also occur inside, causing the lithology around the fractured area to change as well. It can be seen that the cracking and crack propagation of the rock begins to occur at the initial contact moment, and the results captured by the infrared thermal imager well capture this characteristic.

Linear temperature distribution pattern

Under the action of single-tooth cutting, the infrared radiation effect of granite fragmentation essentially originates from the variation of the stress experienced[19]. Therefore, if the data recorded by the infrared thermal image can be extracted, properly processed and analyzed, and compared with the traditional macroscopic force parameters, it would be possible to explore and reveal the damage evolution law of granite from the perspective of combining traditional mechanics and thermodynamics. Therefore, the infrared thermal imager recorded the entire process of different rake angles of the PDC cutter cutting granite. As illustrated in Fig. 8, comparison images are presented to juxtapose the infrared thermal manifestations of the cutting process with experimental measurements acquired during field testing.

Figure 8 is divided into two columns, each containing four sets of corresponding data, used to compare the appearance and infrared thermal imaging characteristics of different rock samples. The left column shows the appearance of the rock, displaying four rock samples labeled with different numbers. The rock surface presents a rough granular structure, and there are subtle differences in texture and color among the different samples, which reflect the material and structural characteristics of the rock itself.

The right column shows the infrared thermogram, which uses color gradients such as purple, green, yellow, and red to present temperature distribution. The closer the color is to red, the higher the temperature is. Each thermal imaging image corresponds to a rock sample in the left column, and different temperature field shapes can be observed in the image, including the location, range, and color density of high-temperature areas. These thermal imaging results intuitively reflect the heat distribution of rocks during the process of action. By comparing the images in the left and right columns, the correlation between different rock materials, structures, and thermal behavior can be analyzed, providing a basis for studying the cutting process of rocks.

From the graphical results, the entire process of linear cutting with PDC cutter, the infrared signal is highly active, accompanied by fluctuations in temperature rise and fall, resulting in varying degrees of rock fragmentation. In the cutting tests conducted on-site, as the rake angle increases, the corresponding fragmentation becomes more severe, accompanied by strong vibrations and explosive sounds.

To research the changes in rock properties throughout the cutting process and the potential evolution of damage, a more detailed analysis is required. In the integrated thermal imaging software IRBIS, the linear temperature distribution results on the surface of granite formed by cutting with four different rake angles were extracted, as shown in Fig. 9. Due to the uniqueness of single tooth cutting, its cutting speed is fast, and the load fluctuates significantly during the cutting process. The feedback between cutting force and infrared temperature is complex and intense, making it extremely difficult to accurately capture specific time nodes. In view of this, author selects the inflection points where significant changes occur during the loading and unloading processes as the distinguishing criteria (i.e. stages A, B, and C in the Fig. 9), and then analyzes the rock failure law. This processing method to some extent overcomes the difficulty of determining time nodes and provides an effective way to reveal the failure mechanism of rocks under single tooth cutting.
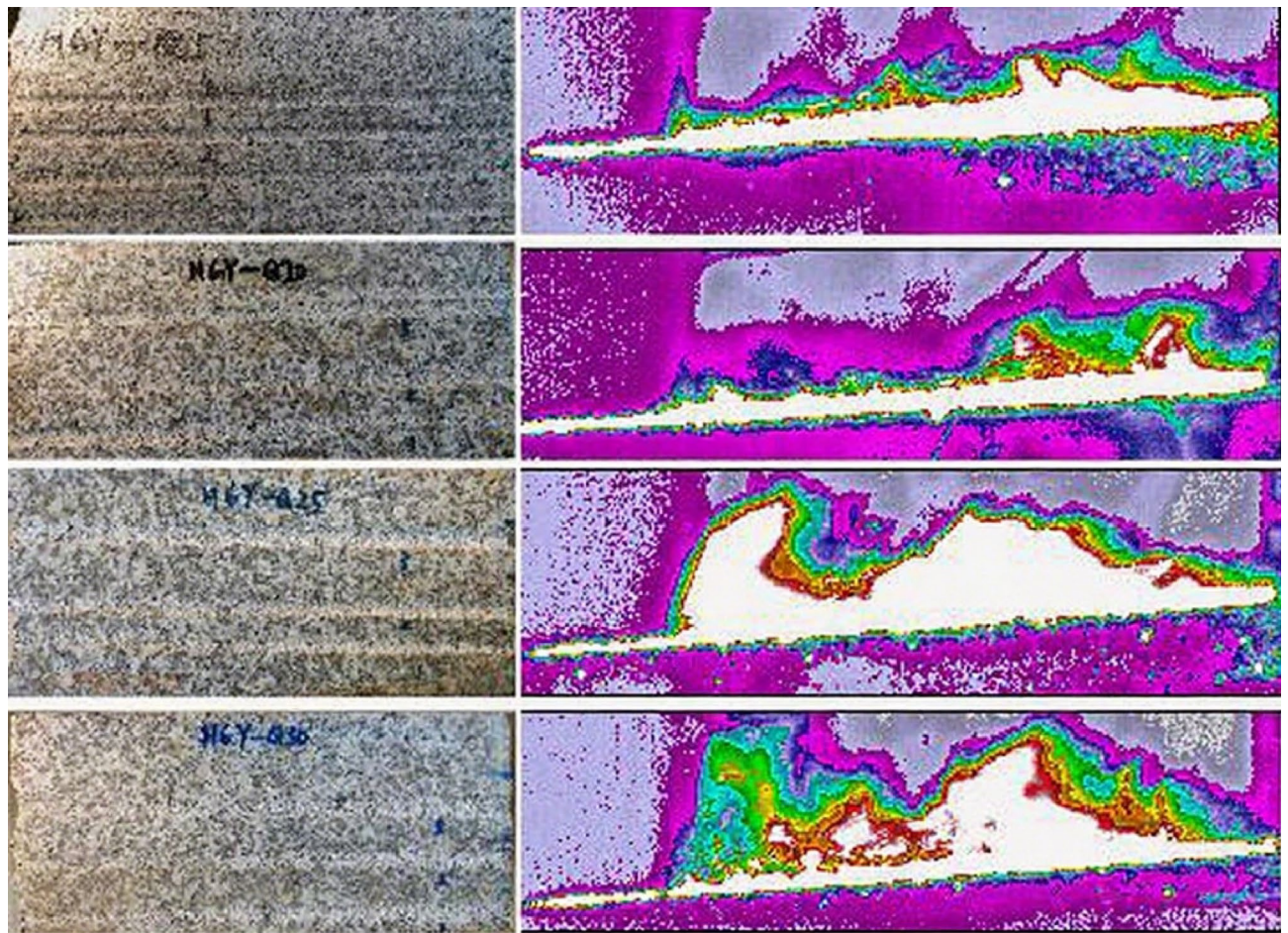
Fig. 8. Infrared signal of rock surface during PDC cutter cutting.

As shown in Fig. 9(a), under the condition of the rake angle of 15°, the overall trend of infrared temperature change is significant. In interval A, the temperature remains around 20 °C. This indicates that at the early stage of the experiment, the infrared temperature change in response to initial conditions is not significant. Upon entering interval B, the temperature rises rapidly, and the fluctuation amplitude increases significantly, reaching a peak of 130 °C around 0.5s, which may imply that within this temperature range, the internal heat exchange or energy conversion process of the system becomes more complex. In interval C, the temperature reaches a relatively high level, showing an overall downward trend.

In comparison, under the condition of the rake angle of 20°, the overall trend of infrared temperature change appears relatively gentle. In interval A, the temperature rises slowly with the small fluctuation amplitude, but compared to the condition of the rake angle of 15°, the temperature rises to 40 °C. Upon entering interval B, the temperature rises significantly, and the fluctuation amplitude remains at a high level, with two peak values appearing. In interval C (around 100 °C), the temperature fluctuates within a small range, without showing a stable downward trend as seen at the rake angle of 15°.

Under the condition of the rake angle of 25°, the overall trend of infrared temperature change is very significant, and it exhibits a back-and-forth fluctuating phenomenon in interval B. The temperature fluctuation in interval A is similar to that at the rake angle of 20°, with a small peak appearing, indicating that interval A is sensitive to temperature changes. The temperature in interval B fluctuates significantly, with the fluctuation amplitude maintaining at about 40 °C ~ 130 °C, showing high sensitivity to temperature changes. The temperature in interval C also fluctuates, but the overall temperature level is similar to that at the rake angle of 20°.

Under the condition of the rake angle of 30°, the temperature change trend in each region is similar to that under the condition of the rake angle of 25°, but in interval B, the back-and-forth fluctuation phenomenon is different from that under the condition of the rake angle of 25°. The temperature fluctuation in interval A is similar to that at the rake angle of 20°, and there are two peak values, indicating that interval A is sensitive to temperature changes. The temperature in interval B also shows reciprocating fluctuations, but the fluctuation amplitude is between 30 °C ~ 130 °C, showing that the region is very sensitive to temperature changes. In interval C, the temperature reaches a relatively high level, about 130 °C, and then drops rapidly, showing an overall downward trend.

By comparing the trends of change under the four conditions, it can be found that the rake angle has a significant impact on the change of infrared temperature. At a lower rake angle (15°~20°), the change in infrared

a) 15 degrees

b) 20 degrees

c) 25 degrees
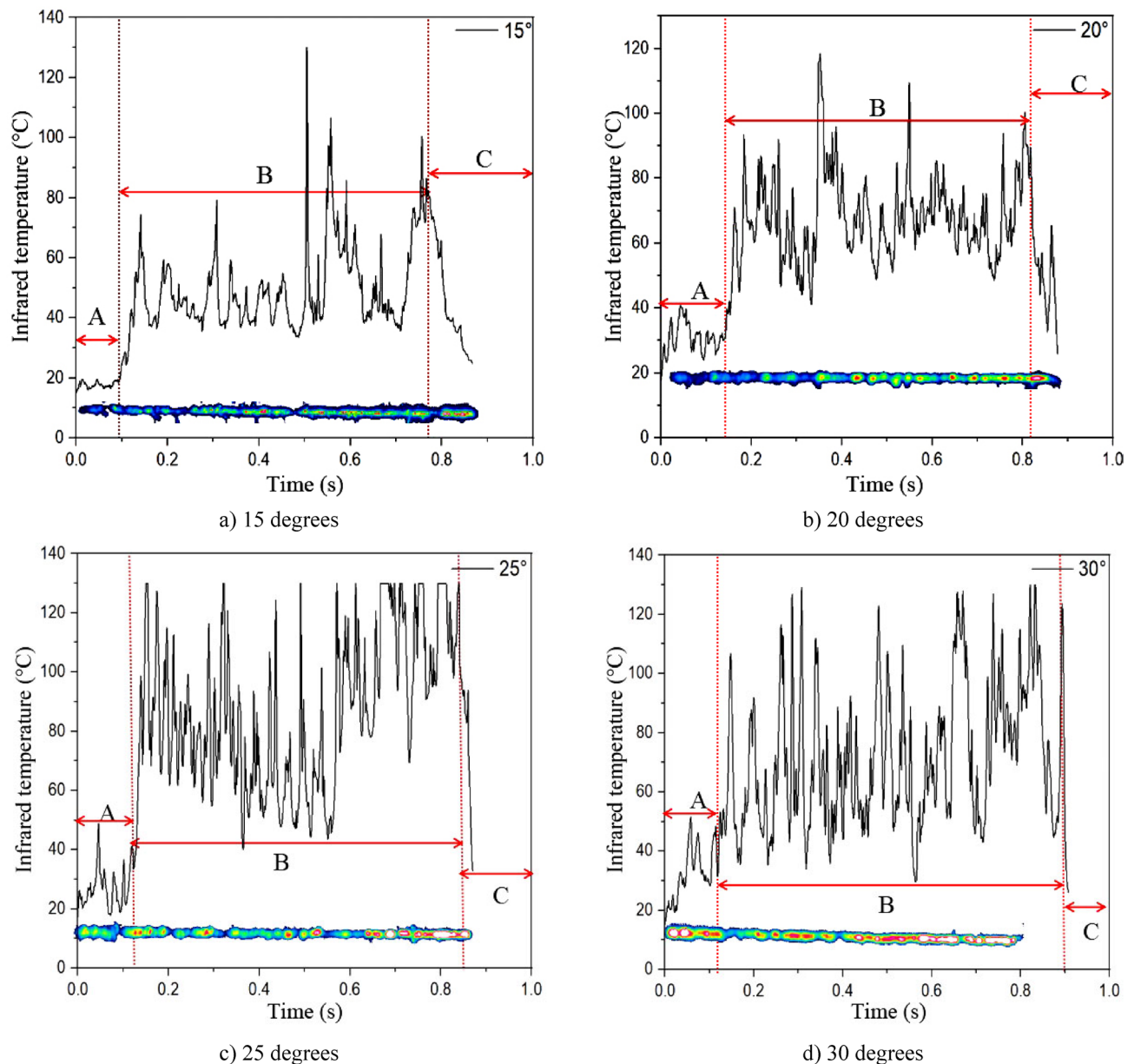
d) 30 degrees

Fig. 9. Line temperature distribution diagram of the cutting process with different rake angles. (a) 15 degrees (b) 20 degrees (c) 25 degrees (d) 30 degrees.

temperature is relatively gentle, with a small fluctuation amplitude. While at a higher rake angle (25°~30°), the change in infrared temperature is more drastic, with a larger fluctuation amplitude. This difference arises from the different thermodynamic behavior or energy conversion efficiency within the system at different rake angles. As the ambient temperature rises, the temperature fluctuation patterns in various regions do not change significantly, but the overall temperature level increases. This indicates that the ambient temperature has a certain impact on the change of infrared temperature, but there are differences in the sensitivity of each region to temperature changes. Interval A is relatively stable, with small temperature fluctuations. Interval B is the most sensitive, being the most affected by temperature changes. Interval C is the most stable, showing an overall downward trend in temperature. At the same time, when the PDC cutter cut granite, as the modified shaper testing machine operates, the infrared radiation reaction occurs instantly at the moment the tooth starts to contact the granite until the cutting ends. The main reasons can be attributed to the following points:

(1) The PDC cutter in contact with granite will produce a frictional heating effect, as the cutting process is very rapid, and the temperature change is also relatively severe.

(2) The granites are a type of heterogeneous and anisotropic substance, and the internal structure of natural granites is very complex, with numerous tiny pores. During the cutting process, under the action of external loads, the internal pores of the granites will undergo a process from closing to compacting and eventually

fracturing. We attribute this phenomenon to the effect of pore gas resolution and escape. This process also releases heat outward.

(3) As the cutting progresses, the cracks generated by granite breakage will also spread to the surrounding areas in varying degrees, a phenomenon we attribute to the crack propagation effect.

For PDC cutters with different rake angles, the temperature field starts to show a fluctuating rise from the contact between the cutter and the granite, repeating this pattern until the cutting process ends, marked by the final cliff-like drop in infrared temperature, after which it will gradually cool to room temperature. The study divides the infrared radiation temperature changes undercutting into the following three stages.

The temperature field evolution during the cutting process of PDC cutters with different rake angles shows significant stage characteristics[20,21]. From the moment the cutting teeth come into contact with the rock, the temperature rises in a nonlinear fluctuating manner with frictional work. This dynamic process continues until the end of cutting, when an infrared temperature measurement signal drops sharply, and then enters the natural cooling stage. This study is based on the research results on cutting friction heat generation, pore gas desorption, and crack propagation effects (references[1,12,15] revealed the macroscopic mechanical energy evolution mechanism of rock fragmentation through uniaxial compression experiments), and innovatively constructed a thermal mechanical coupling analysis model. By synchronously collecting cutting force and infrared radiation temperature data, the temperature variation characteristics and mechanical response of single tooth cutting were correlated and analyzed, and the thermodynamic evolution law of granite fragmentation was systematically revealed. The study divides the cutting process into three typical stages. During the energy accumulation stage, the rapid accumulation of frictional heat in the cutting contact area leads to a sudden temperature rise. In the mixed failure stage, thermal mechanical coupling causes crack propagation and plastic deformation, and temperature fluctuations intensify. During the unloading phase, cracks penetrate and cause sudden stress release, resulting in a sharp decrease in temperature field and accompanied by residual thermal diffusion. This multi parameter collaborative analysis method effectively overcomes the systematic error of single temperature measurement through thermal mechanical bimodal verification, and its core value lies in establishing a quantitative relationship between temperature peak and crack propagation rate. The rock deformation during the three typical stages of the cutting process is as follows.

(1) Energy Accumulation Stage (A). Under the cutting action of the PDC cutter, the granite is compacted and densified in a short time. During this period, the original fissures and pores in the granite will close, and the loss of gas will carry away the internal heat of the granite. At the same time, debris accumulation gradually forms at the contact end between the tooth and the granite.

(2) Mixed Destruction Phase (B). Under the action of single-cutter cutting, the elastic deformation of the granite is extremely weak, and the elastoplastic region runs through the entire cutting process. The B-C phase is the main destruction phase of the granite, where internal micro-cracks rapidly open and spread circumferentially. The destruction is dominated by frictional heating effects and thermo-elastic effects, ultimately leading to a sudden change in the infrared temperature curve.

(3) Unload Phase (C). After experiencing a certain time increment, the granite fragmentation tends to stabilize, after which the granite's breaking gradually becomes gentle under the cutting action, with deformation mainly extending along the completed fracture zone. In this phase, there is almost no generation of new cracks, hence the infrared temperature gradually cools and unloads, and the cutting process ends accordingly.

Multi-index coupling evaluation analysis based on infrared radiation characteristics, dynamic response of cutting force, and SERF

Further analysis reveals that the curve trend presented by the linear temperature distribution pattern shares many similarities with the cutting force curve statistics from conventional cutting experiments. By comparing and analyzing the experimental data of the two, the image of the infrared temperature and the cutting force change process is obtained, as shown in Fig. 10.

Figure 10 systematically reveals the infrared temperature variation phenomenon of granite fracture and its coupling mechanism with mechanical behavior during the PDC cutter cutting of granite through synchronous monitoring data of infrared temperature (red curve) and cutting force (blue curve) at four different rake angles (15°, 20°, 25°, 30°). The horizontal axis represents the cutting position (mm), the left vertical axis is the infrared temperature (°C), and the right vertical axis is the cutting force (N). Each image exhibits significant periodic fluctuation characteristics, indicating that the cutting process consists of a series of "loading-unloading" cycles, directly corresponding to the dynamic evolution process of "compaction-fracture" within the rock. Among them, cutting force refers to the force exerted by PDC single teeth on the rock in the cutting direction when cutting granite. This reflects the active force during the cutting process, that is, the cutting action of the cutting teeth on the rock. The peak value of cutting force corresponds to the loading phase, during which the cutting teeth are actively breaking the rock, which undergoes compaction and fracturing processes. Negative cutting force represents the reactive force encountered during cutting or the resistance of rocks to cutting teeth. This also indicates the unloading stage of gear teeth when passing through materials that have already ruptured or have low resistance.

In the initial cutting stage (the rake angle is 30°), the infrared temperature curve shows high-frequency severe fluctuations, with the temperature varying between 20 °C and 130 °C. In the initial cutting stage (0~50 mm position), the temperature rapidly rises to a peak, corresponding to the elastic deformation stage of the rock. As cutting progresses (50~150 mm position), multiple peaks and valleys appear in the temperature, reflecting the initiation, propagation, and penetration of internal cracks in the granite. Each peak corresponds to a local granite breakage event, with the sudden rise in temperature stemming from the rapid conversion of mechanical energy to thermal energy. In the later cutting stage (150~200 mm position), the temperature fluctuation amplitude
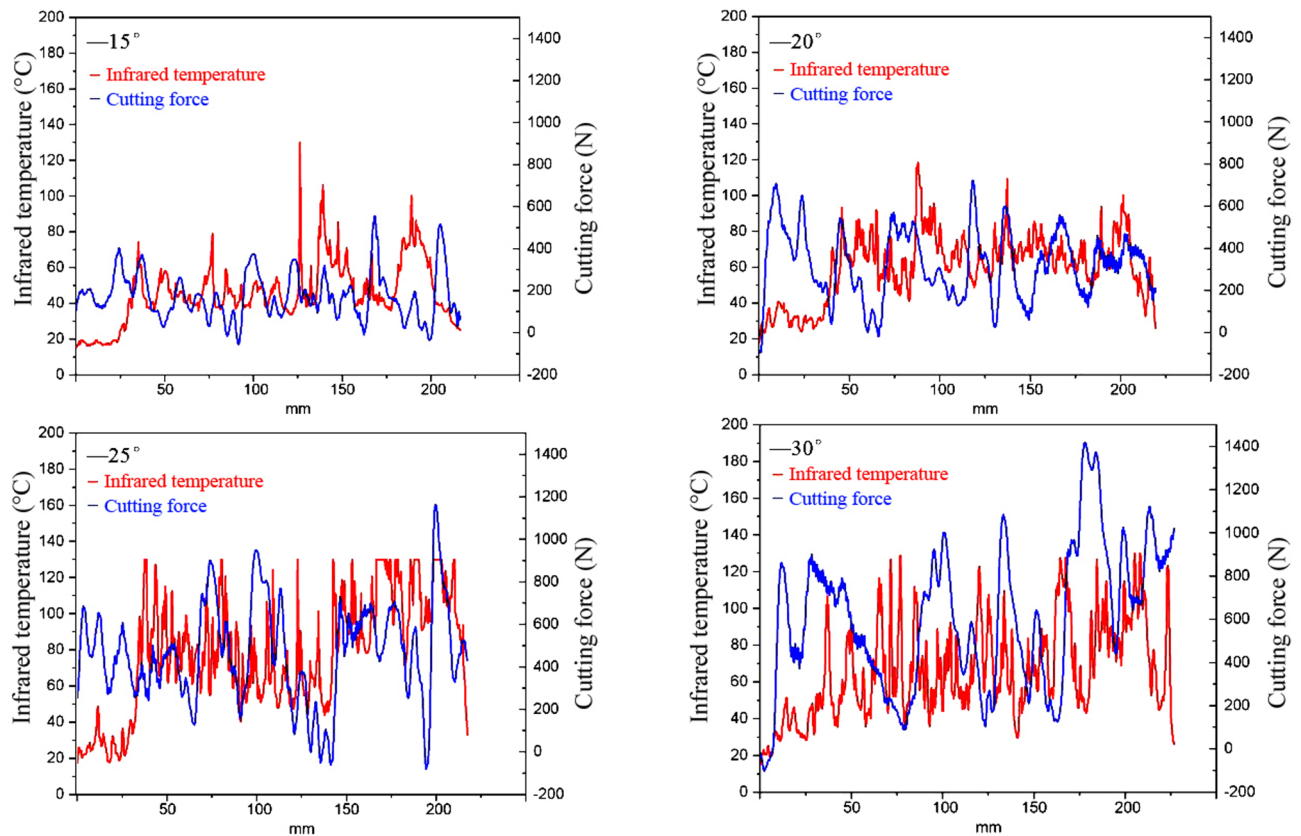
Fig. 10. Infrared temperature versus cutting force. Please replace Figure 10, as the numbers on the right side of the original Figure 10 are not fully displayed.

decreases, indicating that rock fragmentation gradually stabilizes, which may be related to the cumulative granite damage leading to a decrease in strength.

The cutting force curve fluctuates in a trend highly similar to the infrared temperature, but with a larger variation amplitude (0 ~ 1400 N). In the initial cutting stage, the cutting force gradually increases. It reached the first peak (approximately 800 N) near the 50 mm position. Then it rapidly declined, corresponding to the first severe granite fracture. Afterward, the cutting force exhibits periodic fluctuations, with each peak (such as at the 100 mm and 150 mm positions) corresponding to a significant granite fracture event. Near the 180mm position, the cutting force reaches its highest value (about 1400 N). Throughout the cutting process, there is repeated vibration, which is related to the ejection of granite fragments or the intermittent contact between the cutter and the granite.

The synchronous fluctuation of infrared temperature and cutting force verify the thermo-mechanical coupling mechanism of granite fracture. In the peak area of cutting force, the infrared temperature reaches its peak simultaneously, indicating that mechanical energy is efficiently transformed into thermal energy through crack propagation and particle friction. For instance, at around the 130 mm position, when the cutting force reaches 1100 N, the corresponding infrared temperature rises to 110 °C, and this energy conversion efficiency directly reflects the intensity of the granite. Moreover, the fluctuation frequency of the temperature curve is consistent with the cutting force fluctuation period, indicating that rock fracture has significant periodic characteristics, with each period corresponding to a "loading-unloading" cycle, directly corresponding to the dynamic process of granite compaction and fracture. By comparing different conditions of rake angles, it is evident that the rake angle significantly affects the energy distribution and temperature fluctuation characteristics during the granite breaking process. At a 15° rake angle, the peak of cutting force is lower (about 600 N) and the infrared temperature fluctuation amplitude is larger (peak temperature about 130 °C), indicating that granite fragmentation is mainly slow brittle fracture. While the rake angle increases to 20°, the peak rises to about 700 N, and the temperature fluctuation amplitude decreases to about 120 °C, reflecting that the increase in rake angle intensifies the degree of rock fragmentation and produces some energy release. As the rake angle increases to 25°, the peak of cutting force significantly rises to 1100 N, and the temperature fluctuation amplitude remains at about 130 °C, reflecting that the increase in rake angle intensifies the degree of rock fragmentation, leading to energy release. When the rake angle increases to 30°, the peak of cutting force reaches about 1400 N, and the temperature fluctuation amplitude remains at about 130 °C, reflecting that the increase in rake angle intensifies the degree of granite fragmentation, resulting in more severe energy release, but the peak temperature remains stable.

Therefore, the periodic characteristics of infrared temperature variation are closely related to the micro-mechanism of granite fracture. In each "loading-unloading" cycle, the granite undergoes stages such as

Rake angle	Range	Mean	Variance
15°	115.31	58.06	14.46
20°	110.37	53.76	17.10
25°	112.78	45.82	20.13
30°	111.32	39.54	21.34

Table 5. Statistical results of infrared characteristic temperature under different rake angles. Note: All units are in Celsius °C.
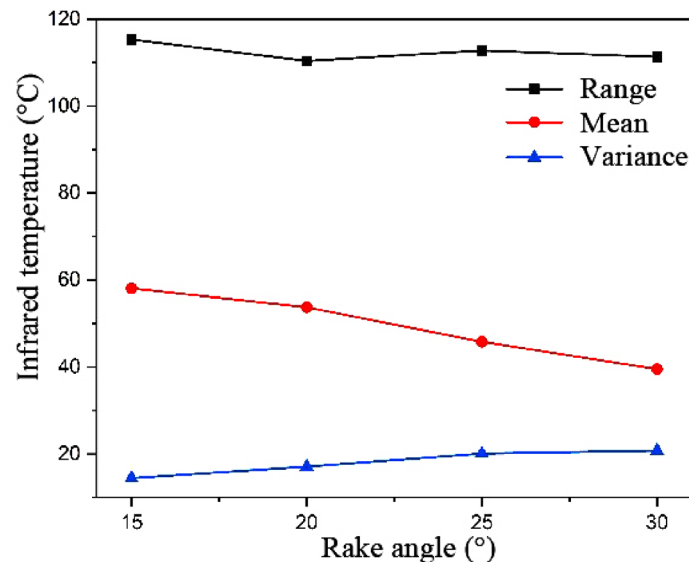
Fig. 11. Several kinds of infrared temperature statistics under different rake angles.

compaction, crack initiation, propagation, and penetration. The cutting center area experiences severe fragmentation due to stress concentration. As a result, the infrared temperature rises. The circumferential diffusion area is mainly characterized by micro-crack propagation, with the smaller temperature fluctuation amplitude. This spatial heterogeneity is manifested in the infrared image as a temperature gradient distribution from the contact center to the edge, which highly matches the spatial evolution pattern of granite damage degree.

At the same time, in order to research the infrared characteristic temperatures of several types under different rake angles, the range, mean, and variance of the infrared temperature field under different rake angles were extracted. As shown in Table 5, the curve data was plotted as shown in Fig. 11.

From the data statistics in Table 5, the range of variation for the four types of rake angles is not significant. The variation range is between 115.31 °C ~ 110.37 °C, with an absolute change rate of 4%. However, the average temperature and variance calculated under the four types of tilt angles show certain differences.

Figure 11 shows the relationship between different rake angles (15° ~ 30°) and infrared temperature in range, mean, and variance. These parameters quantify the distribution characteristics and fluctuation properties of the temperature field during PDC cutting from different perspectives, revealing the influence of the rake angle on the thermal effects of granite breaking.

The range reflection indicates the maximum fluctuation range of the infrared temperature, which represents the severity of temperature changes during the cutting process. Data show that as the rake angle increases from 15° to 30°, the range first slightly decreases and then slightly rises. While the rake angel is 15°, the range is 115.31 °C, dropping to 110.37 °C at 20°, rising to 112.78 °C at 25°, and 111.32 °C at 30°. This change indicates that the influence of the rake angle on the temperature fluctuation amplitude is not a monotonic linear relationship. In the 15° ~ 20°, the decrease in the range may be due to the change in granite breaking mode caused by the increased rake angle, transitioning from severe brittle fracture to more sustained wear, reducing instantaneous high-temperature events. In the 25° ~ 30°, the rise may be due to excessive rake angle leading to increased local stress concentration, causing more frequent severe fractures, thus expanding the temperature fluctuation range.

The mean value characterizes the overall energy level of the infrared temperature. The data shows that the mean exhibits a monotonically decreasing trend with the rake angle increase. While the rake angel is 15°, the mean is 58.06 °C, then, dropping to 53.76 °C at 20°, further dropping to 45.82 °C at 25°, and reaching the lowest value of 39.54 °C at 30°. This trend indicates that an increased rake angle leads to more uneven energy distribution in the cutting process, with high-temperature areas possibly more concentrated at local contact points, while the overall average temperature decreases instead. Possible mechanisms include more intense granite fragmentation

under a larger rake angle, with rapid debris removal leading to reduced heat accumulation, or a larger rake angle causing cutting heat to be more easily dissipated through the interface between the PDC cutter and the granite.

The variance reflects the dispersion degree of the infrared temperature, i.e., the uniformity of the temperature distribution. Data show that variance exhibits a significant upward trend as the rake angle increases. It is 14.46 °C at 15°, increases to 17.10 °C at 20°, reaches 20.13 °C at 25°, and rises to 21.34 °C at 30°. This trend indicates that an increased rake angle leads to a less uniform temperature field distribution, with an increase in local high-temperature areas. By combining the changes in the range and mean, with the larger rake angle, granite fragmentation is more intense, but the fragmentation process presents stronger non-uniformity, causing energy to be released in a concentrated manner in space, forming local high-temperature hotspots, while the overall average temperature decreases due to thermal diffusion or debris exclusion.

Therefore, the rake angle has a significant regulatory effect on the thermal effects of the rock-breaking process. At a smaller rake angle (15° ~ 20°), the granite breaking process is relatively mild, with larger temperature fluctuations, but the overall energy level is higher and the temperature distribution is more uniform. At a larger rake edge angle (25° ~ 30°), the granite breaking process is more intense, with a slight increase in temperature fluctuation amplitude, a lower overall energy level, but the temperature distribution is extremely uneven, with a significant increase in local high-temperature areas. From a thermo-mechanical coupling perspective, although a larger cutting edge angle can improve rock-breaking efficiency, it leads to more intense local thermal shocks on the PDC cutter, accelerating thermal fatigue damage, which is consistent with the experimental results of previous studies showing that cutting force and crushing specific work increase when the rake angle exceeds 25°. In PDC cutter design, it is necessary to balance granite breaking efficiency and its life, choosing an appropriate rake angle range (such as 15° ~ 25°) to achieve the best balance of efficient granite breaking and PDC cutter durability.

Simultaneously, as the rake angle increases, the PDC cutter's ability to cut into the granite becomes stronger, leading to a more intense rock -breaking process and more frequent fluctuations. Research has found that the infrared temperature change precursors of granite fracturing can be summarized into two categories, sudden rise and sudden fall. For rocks with greater hardness like granite, as the rock-breaking behavior becomes more intense, the brittle fragmentation is particularly significant, leading to the release of heat. Therefore, as the rake angle increases, the mean value generally shows a downward trend. The statistical data of variance show a positive correlation with the cutter's rake angle, indicating that as the rake angle increases, the fluctuations in infrared temperature become more frequent, and the rock-breaking behavior is more intense. However, in practical applications, a larger rake angle is not always more beneficial for granite breaking, hence the introduction of crushing specific work and cutting load for further quantitative analysis.

Currently, for single-tooth granite breaking, the SERF is usually expressed as the energy consumed to break a unit volume of rock, which can be divided into two types, projected breaking volume and actual breaking volume. This paper uses the actual breaking volume for calculation, as Eq. (1).

$$SERF = \frac{E}{V} = \frac{FL}{V} \tag{1}$$

Here, *SERF* represents the specific energy of rock fragmentation. *E* represents the energy consumption for rock breaking. *F* represents the tangential force. *L* represents the displacement of linear cutting. *V* represents the actual rock breaking volume (cuttings).

In the actual experimental process, in order to ensure the integrity of rock debris collection, this study systematically considered and optimized the design for possible debris splashing and incomplete collection caused by other factors. Specifically, the author innovatively installed a protective device on the rock placement base. The device adopts a three sided enclosed structure, which accurately covers the other three non-machined surfaces of the rock except for the cutting surface, and a chip collection groove is scientifically set at the tail of the device. During the experiment, the rock debris generated by cutting slides down the inner wall of the protective cover under the action of gravity, and eventually gathers in the predetermined groove. For a small amount of residual rock debris attached to the rock surface, a special soft bristled brush is used for secondary fine collection. Through the organic combination of this two-stage collection mechanism and splash proof design, the collection error of rock debris is effectively controlled within a very small range, laying a reliable foundation for the accurate analysis of subsequent experimental data.

In this experiment, cutting operations were carried out by setting the tool rake angle parameters, and the granite debris generated under various rake angle conditions was collected. The morphological characteristics of the debris are shown in Fig. 12. The collected rock fragments are used as key samples for precise calculation of SERF. After completing the SERF calculation, systematically compare and analyze the obtained SERF values with the tangential and axial force data measured synchronously during the experimental process. Finally, the results of the comparative analysis are shown in Fig. 13.

Figure 13 shows the trend of the influence of different rake angles (15° ~ 30°) on SERF (MPa), tangential force (N), and axial force (N) during the PDC single-tooth cutting of granite. By analyzing the variation patterns of these parameters, the regulatory mechanism of the rake angle on rock-breaking efficiency and mechanical behavior is researched.

SERF increases monotonically with the increase of the rake angle. At 15°, SERF is at its lowest value, and it increases significantly as the rake angle increases to 30°. This trend indicates that the increase of rake angle leads to increased difficulty in rock-breaking, and the energy required for breaking the unit volume of granite rises. The physical mechanism may be related to the change in rock-breaking mode caused by the increase in the rake angle. As the rake angle is smaller, 15° ~ 20°, the granite mainly breaks by brittle fracture and consumes less
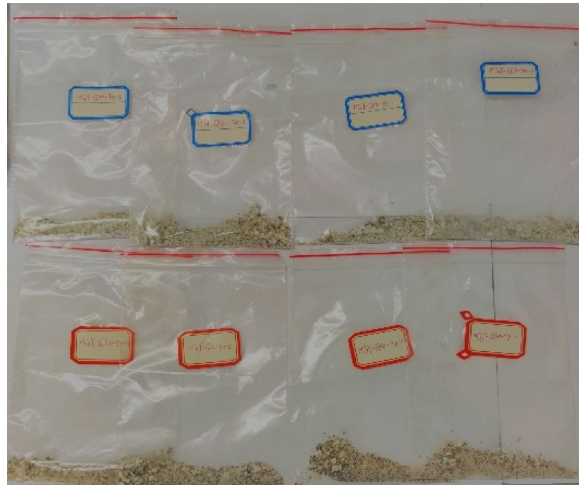
Fig. 12. Morphological characteristics of the granite debris.
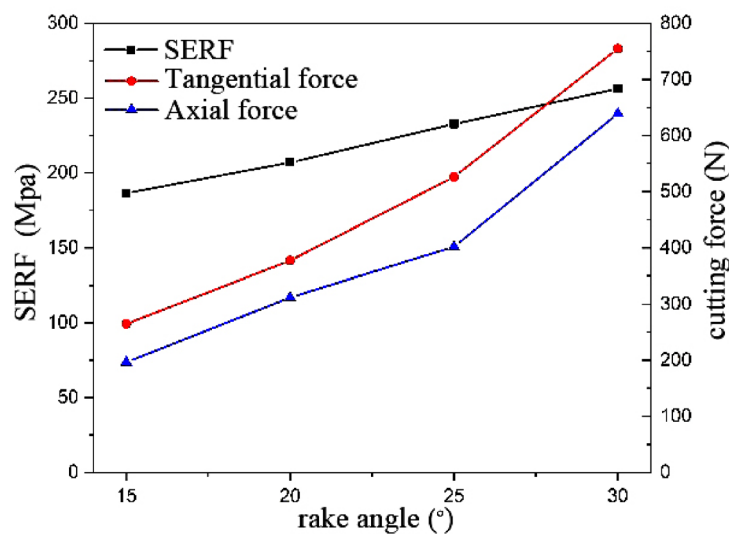
Fig. 13. SERF and cutting force with different rake angles.

energy. As the rake angle is larger, 25° ~ 30°, the granite may undergo local plastic deformation or multiple crack propagation, resulting in increased energy dissipation.

The tangential force shows a significant upward trend as the rake angle increases, especially after 25°, where the increase intensifies. At 15°, the tangential force is at a lower value, and it rises sharply when reaching 30°. This trend reflects that the increase in the rake angle leads to a sharp increase in the horizontal resistance of the granite against the PDC cutter. The causes may include that under a larger rake angle, the contact area between the PDC cutter and the granite increases, leading to a rise in frictional resistance. At the same time, the granite breaks more violently, producing more debris, which further exacerbates the fluctuation of the tangential force. It is worth noting that the steep increase in tangential force after 25° may indicate a qualitative change in the granite-breaking mechanism, such as a shift from brittle fracture to plastic fracture.

The axial force shows a slow upward trend as the rake angle increases, with the overall change amplitude being less than the tangential force. At 15°, the axial force is at its lowest value, gradually increasing to 30°. This trend indicates that an increased rake angle leads to deeper penetration of the PDC cutter into the granite, but the increase is relatively limited. Possible mechanisms include that the increased rake angle causes an increase in the normal stress component of the PDC cutter, thereby enhancing the axial force. However, the granite's compressive strength limits the excessive growth of the axial force.

By combining the trends of SERF, tangential force, and axial force, the following conclusions can be drawn. The rake angle has a dual impact on the granite breaking process. On the one hand, increasing the rake angle can enhance the SERF, indicating improved granite breaking efficiency. On the other hand, a significant increase in tangential force and axial force can lead to intensified PDC cutter wear and increased energy consumption. There is a critical inclination angle (approximately 25°), beyond which the tangential force rises sharply, possibly

causing intensified PDC cutter vibration and enhanced thermal shock, adversely affecting the lifespan. In practical applications, it is necessary to balance granite breaking efficiency and PDC cutter lifespan, with a smaller rake angle (15° ~ 20°) suitable for soft granite formations to reduce wear. A larger rake angle (25° ~ 30°) is suitable for hard granite formations to improve breaking efficiency, but requires the matching wear-resistant cutter and an efficient cooling system. Therefore, by reasonably adjusting the rake angle, the granite breaking process can be optimized to achieve a balance between efficient drilling and cutter durability. Based on the research background of this paper, it is recommended to control the PDC cutter's rake angle within the range of 15° ~ 25°.

Conclusions

This paper conducts experimental research on the infrared radiation characteristics, damage evolution of PDC cutter cutting granite using the modified shaper testing machine, and the infrared thermal imaging monitoring system. The following conclusions are drawn.

(1) While the PDC cutter contacts the granite, it produces drastic infrared temperature changes, which can characterize the fracturing of the granite. As the rake angle increases, the contact temperature between the two changes within a higher temperature range, adversely affecting the cutter's lifespan. Combined with the results of infrared imaging, the fracturing of the granite is not only reflected in the central contact area but also spreads to its surroundings. The granite also undergoes complex structural changes internally, altering the properties of the rock around the fractured area.

(2) In this study, the infrared radiation temperature evolution characteristics of rocks under cutting action were carefully divided into three key stages: energy accumulation stage, mixed failure stage, and unloading stage. By utilizing the infrared thermal response characteristics, it is possible to effectively determine the internal failure state of rocks at different times, providing a perspective and basis for a deeper understanding of the failure mechanism of rocks during cutting processes.

(3) Under the condition of the cutting depth of 1.5 mm set in this study, when the rake angle of PDC cutter exceeds 25 °, the calculated results of infrared radiation response, cutting load, and crushing specific energy during the cutting process show varying degrees of increase. The enhancement of infrared radiation response may imply a change in energy dissipation in the cutting area. An increase in cutting load will increase the burden on the equipment, while an increase in crushing specific work reflects the change in cutting efficiency. Based on the research background of exploring the cutting characteristics of PDC teeth and optimizing cutting parameters in this article, considering multiple aspects such as ensuring the stability of the cutting process, controlling energy consumption, and improving cutting efficiency, it is recommended to control the rake angle of PDC cutter within the range of 15 ° ~ 25 °.

Data availability

References

1. Dongming Zhang, Shuaida Zhu, Mingliang Zhou, Hongwei Huang and Yue Tong. Damage quantification and failure prediction of rock: A novel approach based on energy evolution obtained from infrared radiation and acoustic emission. *Int. J. Rock Mech. Min. Sci.* **183**, 105920–105920 (2024).
2. Changfeng Li, Chunlu Lan, Baokun Zhou, Chaoyang Zhu, Qiru Sui, Xiaolin Hou and Chunlai Wang. Infrared temperature distribution characteristics and state assessment method of sandstone under tension and compression stress. *Infrared Phys. Technol.* **142**, 105549–105549 (2024).
3. Qiangqiang Gao, Liqiang Ma,Wei Liu, Hui Wang, Qiang Ma and Xiuzhe Wang. Identification of damage states of load-bearing rocks using infrared radiation monitoring methods. *Measurement* **239**, 115507–115507 (2025).
4. Xin Cai, Jifeng Yun, Zilong Zhou, Yunming Wang, Liye Chen, Yang Liu and Shaofeng Wang. Strain rate-dependency of thermal infrared radiation of sandstone subjected to dynamic loading: insights from a lab testing. *Int. J. Rock Mech. Min. Sci.* **181**, 105855 (2024).
5. Longfei Chang, Lu Chen, Mingyuan Zhang, Dejian Li and Yingjun Li. Experimental study on infrared radiation and crack evolution characteristics during the failure process of rocks with pre-set crack. *Infrared Phys. Technol.* **138**, 105236 (2024).
6. Jianwei Huang, Shanjun Liu, Chunju Zhang, Jinchao Li, Jun Geng, Shuiping Li, Min Yu and Chaoqun Chu. Thermal infrared spectrum variation and waveband features of loaded rocks with different mineral components during the fracture evolution process. *Infrared Phys. Technol.* **137**, 105120 (2024).
7. Liqiang Ma, Naseer Muhammad Khan, Tariq Feroze, Mohammed Sazid, Kewang Cao, Sajjad Hussain, Qiangqiang Gao, Saad S. Alarifi and Hui Wang. Prediction of rock loading stages using average infrared radiation temperature under shear and uniaxial loading. *Infrared Phys. Technol.* **136**, 105084 (2024).
8. Wei Liu, Liqiang Ma, Qiangqiang Gao, Anthony John Spencer Spearing, Yangyang Wang, Ruoyu Cui and Zhiyang Zhao. Fracture precursor recognition and damage quantitative characterization of stressed rock using infrared radiation. *Rock Mech. Rock Eng.* **56** (8), 5567–5584 (2023).
9. Bo Li, Yizheng He, Li Li, Junxiang Zhang, Zhen Shi and Yapeng Zhang. Damage evolution of rock containing prefabricated cracks based on infrared radiation and energy dissipation. *Theoret. Appl. Fract. Mech.* **125**, 103853, 1–12 (2023).
10. Qiangqiang Gao, Liqiang Ma, Wei Liu, Naseer Muhammad Khan, Guanghui Cao, Yumiao Fang and Hui Wang. Research on the denoising method of infrared thermogram during rock fracture. *Infrared Phys. Technol.* **131**,104651, 1–10 (2023).
11. Xiaoming Sun, Huichen Xu, Manchao He and Fang Zhang. Experimental investigation of the cccurrence of rockburst in a rock specimen through infrared thermography and acoustic emission. *International Journal of Rock Mechanics and Mining Sciences* **93**, 250–259 (2017).

12. Zilong Zhou, Xin Cai, Xibing Li, Wenzhuo Cao and Xueming Du. Dynamic response and energy evolution of sandstone under coupled static–dynamic compression: insights from experimental study into deep rock engineering applications. *Rock Mechanics and Rock Engineering*, **53** (3), 1305–1331 (2020).
13. Zilong Zhou, Yang Liu, Xin Cai, Yin Chang and Shan Gao. Infrared radiation characteristics of sandstone exposed to impact loading. *J. Cent. South. Univ. (Science Technology).* **53** (7), 2555–2562 (2022).
14. Shunxi Yan, Huangfu Run, Xiaolei Wang, Pengcheng Jiang and Sibo Zhan. Study on infrared radiation characteristics of layered gneiss, *Journal of Henan Polytechnic University (Natural Science).* **41** (2), 156–163 (2022).
15. Huangfu Run, Shunxi Yan, Xiaolei Wang, pengcheng Jiang and Sibo Zhan. Experimental study on infrared radiation characteristics of gneiss under uniaxial compression. *J. Min. Strata Control Eng.* **3** (1), 013011 (2021).
16. Xianzhen Wu, Xiang Gao, Xiangxin Liu and Kui Zhao. Abnormality of infrared temperature mutation in the process of siltstone failure, *Journal of China Coal Society*, **40** (S2): 328–336(2015).
17. Yanbo Zhang, Jian Li, Xiangxin Liu, Baozhu Tian and Shanjun Liu. Influence of water on infrared radiation characteristic of granite roadway rock burst. *J. Liaoning Tech. University: Nat. Sci.* **34** (4), 453–458 (2015).
18. Yueyu Lei, Zhonghui Li, Tian He, Aikeremujiang Aihemaiti, Xueli Li and Quan Lou. Experimental study on changes of infrared radiation energy in siltstone failure process under different loading rates. *Saf. Coal Mines.* **55** (1), 151–159 (2024).
19. Han Xie, Yuchun Kuang and Chao Qin. The finite element simulation and test of rock breaking by non-planar PDC cutting cutter. *Petroleum Drill. Techniques.* **47** (5), 69–73 (2019).
20. Guanghui Zhu, Yuchun Kuang and Wei Lin. Research on cutting load and heat generation law of PDC wearing cutter. *China Petroleum Mach.* **49** (5), 68–73 (2021).
21. Li Hu, Yuchun Kuang, Wei Long, Wei Lin and Yiwei Han. Design and rock-breaking mechanism of micro-bit with wide edge cutter. *China Petroleum Mach.* **52** (11), 1–11 (2024).

Acknowledgements

Author contributions

X.J. He. and B. Zheng. wrote the main manuscript text and Z.C. Luo, P.H. Hu. and Y.J. Yang. prepared figures. methodology, B.Z. and G.F. Yin; software, Y. J.Yang; All authors reviewed the manuscript.

Declarations

Competing interests

The authors declare no competing interests.

Additional information

Correspondence and requests for materials should be addressed to B.Z.

Reprints and permissions information is available at www.nature.com/reprints.

Publisher's note Springer Nature remains neutral with regard to jurisdictional claims in published maps and institutional affiliations.